Electronic structure of beryllium fluoride

K. L. Bedford, R. T. Williams, W. R. Hunter,* and J. C. Rife
Naval Research Laboratory, Washington, D.C. 20375

M. J. Weber, D. D. Kingman, and C. F. Cline
Lawrence Livermore National Laboratory, Livermore, California 94550
(Received 19 July 1982; revised manuscript received 7 October 1982)

Vacuum-ultraviolet reflectance, absorptance, and photoelectron spectroscopy of vitreous and crystalline BeF_2 are reported. The data are interpreted with reference to self-consistent unrestricted Hartree-Fock cluster calculations also presented in this paper. The first allowed exciton reflectance peak in crystalline BeF_2 is at 12.9 eV, similar to the 12.8-eV peak found in the glass. Optical transmission of bulk samples extends at least to 9.5 eV, and can be assumed to be impurity limited in available material. Calculations of several defect and impurity levels are presented. Since the calculations presented here indicate that BeF_2 should have an optically forbidden band edge similar to that in SiO_2, the ultimate transparency range of purified BeF_2 will depend on the forbidden exciton absorption, not yet observable above the impurity background. Grazing-incidence reflectance spectra near the Be^{2+} K edge are interpreted in terms of a core exciton state lying at or slightly below the conduction-band minimum as determined from x-ray photoelectron data and the optical band gap.

I. INTRODUCTION

Beryllium fluoride (BeF_2) is a highly ionic transparent solid which exists in both glassy and crystalline forms isomorphic with SiO_2 structures. The glass is composed of basic BeF_4 tetrahedra analogous to SiO_4 in fused silica. The common crystalline form of BeF_2 exhibits the α-quartz structure. Beryllium fluoride has an extremely low refractive index, $n_d=1.275$ measured in the glass, as compared, for example, with $n_d=1.392$ in crystalline LiF. The visible dispersion, represented by the reciprocal Abbé number

$$\nu^{-1}=\left|\frac{n_F-n_C}{n_d-1}\right|=9.3\times10^{-3}\,,$$

and the nonlinear coefficient of refractive index at 1.06 μm, $n_2=2.3\times10^{-14}$ esu, are also very low when compared with values for other transparent materials.[1] Although principally investigated in connection with fluoroberyllate glasses for high-power laser materials requiring low n_2, beryllium fluoride is also promising as a vacuum-ultraviolet optical material or thin-film component of an optical multilayer stack. Partly because it is both toxic and hygroscopic, however, BeF_2 has not been as well characterized as most other alkaline-earth fluorides.

The unusually low values of refractive index and visible dispersion found in BeF_2 suggest a very large optical gap. A single-oscillator model for solids, as discussed by Wemple and DiDomenico,[2] can be used to relate measured values of n and dn/dE to the energy E_0 of an effective dispersion oscillator. Such an analysis reported in Ref. 3 yielded $E_0=16.5$, 15.7, 15.1, 13.8, and 12.6 eV in BeF_2, LiF, CaF_2, BaF_2, and SiO_2, respectively. This trend is supported by ultraviolet photoelectron spectroscopy (UPS) data from Poole *et al.*,[4] giving binding energies at the peak ($\sim$ centroid) of the UPS valence-band density of states as $E_b=17.2$, 12.3, and 11.0 eV in BeF_2, CaF_2, and BaF_2, respectively. While it seems clear from the above considerations that oscillator strength near the optical gap must be peaked at higher energy on the average in BeF_2 than in other common wide-gap materials, the prospect of an optical gap significantly larger than in LiF was not borne out by the first reflectance data,[3] which showed a strong exciton reflectance peak at 12.8 eV in BeF_2 glass. The possibility of a wider optical gap in crystalline BeF_2 is one of the points addressed by experiments reported in this work.

In relating the reflectance data of Ref. 3 to a minimum band gap for BeF_2, two reasonable but mutually exclusive assumptions could be made. The lowest band edge could be either allowed and direct as in most other alkaline-earth halides and alkali halides, or optically forbidden as in the structurally

isomorphic material SiO_2. Both possibilities were raised in Ref. 3. Recent calculations by Bedford[5] showed that in fact the lowest absorption edge should be optically forbidden in BeF_2. Theoretical results and implications for interpretation of the experimental data are discussed below. Additional data on core levels are presented, and features due to impurities are compared to defect cluster calculations.

II. EXPERIMENTAL METHODS

The BeF_2-glass samples were made[6] by heating $(NH_4)_2BeF_4$ powder in a graphite crucible to liberate NH_4F and fuse the remaining BeF_2. An N_2 or CO_2 atmosphere over the melt was found to improve the ultraviolet transmittance of the resulting glass. To prepare crystallized samples used in the present work, pure BeF_2 glass was heated under a nitrogen atmosphere at 500 °C for 500 h, crystallizing the sample in the β-BeF_2 temperature region. The temperature was lowered very slowly through the β- to α-phase transition. A matrix of large grains (1—2 mm) of BeF_2 isomorphic with α-quartz resulted. X-ray diffraction analysis of the polycrystalline sample surface indicated a rather high degree of grain orientation, so that the exposed face was predominantly [100]. The calculated x-ray density of α-BeF_2 was 2.304 g/cm^3 as compared to 1.987 g/cm^3 for the glass. The sample remained near its original size and shape through the glass to crystal transition. Hence contraction due to the density change resulted in large internal voids. Impurities were observed in the grain boundaries and x-ray diffraction indicated that some BeO was present.

The toxicity and hygroscopic nature of BeF_2 are complicating factors in its production and use. The immersion solubility of pure vitreous BeF_2 is less than that of LiF (0.0661 versus 0.225 g/cm^2 in 24 h at 23 °C),[6] but BeF_2 surfaces are found to be more susceptible to attack by atmospheric moisture. Surfaces were polished in SnO_2 and ethylene glycol under dry-box conditions. After preparation at Lawrence Livermore National Laboratory (LLNL), the samples were transported to the Naval Research Laboratory and then to the National Bureau of Standards Synchrotron Ultraviolet Radiation Facility in desiccated containers. Samples were loaded into the vacuum system with a minimum of air exposure, generally less than 20 min. In an effort to clean the surfaces, samples were argon-sputter-etched to a depth of about 30 nm before measurements of reflectivity (from 8—50 eV) and of photoelectron spectra. The initial stages of sputter cleaning produced noticeable sharpening of some features in the reflectance spectrum. However, continued sputtering produced no additional improvement and eventually degraded the sharpness of spectral features. Auger-sputter-profiling has been performed on some of the samples,[3] showing that oxygen and carbon exist at concentrations of about 4 at.% throughout at least the first 100 nm. As expected from the behavior of other halides, sputter-etching caused preferential loss of fluorine from the surface and formation of some Be metal.

The ultraviolet light source used for most of these experiments was the Synchrotron Ultraviolet Radiation Facility (SURF II) at the National Bureau of Standards (NBS). The spectral range from 8—50 eV was covered by a toroidal grating monochromator, and the (40—160)-eV range was covered with a 2.2-m grazing-incidence monochromator. Measurements on crystalline BeF_2 in the (6—24)-eV range were made using the NBS high-intensity normal-incidence monochromator.[7] Transmittance and reflectance measurements in the (4—10)-eV range were also made at LLNL using laboratory sources and a normal-incidence monochromator.

Reflectance measurements were accomplished with a detector which could be positioned to accept the reflected beam, and could then be repositioned, under vacuum, into the incident beam for a determination of incident flux. With the use of normalization of both signals to the storage-ring current, a ratio of reflected to incident flux was obtained. The distance from the sample to the detector was about 5 cm, and the detector area was about 1 cm^2. Three different detectors were used, depending on spectral range and other conditions. For high photon fluxes available in the (16—160)-eV range, an aluminum-surface vacuum photodiode was used. Data between 8 and 16 eV taken with the toroidal-grating monochromator utilized a channeltron electron multiplier as the detector. Reflectance of crystalline BeF_2 in the (6—24)-eV range was measured using an ultrahigh vacuum compatible photomultiplier having a sodium salycilate coating. The normal-incidence monochromator had adequate rejection of higher orders throughout the working range. Numerical corrections for second order determined by photoelectron spectroscopy were made in data from 16—50 eV. Lithium fluoride and indium filters were used for higher-order exclusion below 16 eV.

Photoelectron spectra were measured using a double-pass cylindrical mirror analyzer. Since these were bulk-insulator samples, it was necessary to provide charge neutralization when making photoelectron measurements. This was done by means of a filament serving as a flooding source of low-energy electrons. A current balance is obtained rather than absolute neutralization, so some feature of the spectrum must be established as an energy reference, as discussed below.

III. EXPERIMENTAL RESULTS

A. Vitreous BeF_2

The normal-incidence reflectance spectrum of BeF_2 glass is shown in Fig. 1 along with plots of the real and imaginary parts of the complex dielectric constant $\hat{\epsilon}=\epsilon_1+i\epsilon_2$. The method of Kramers-Kronig analysis employed here uses Lorentzian-broadened oscillators to approximate high- and low-energy extensions of the data.[8] The dashed line in Fig. 1(a) shows the low-energy extension that was made. The polished sample surface was cleaned by argon-sputter-etching, but because of roughness, residual contamination, and/or sputtering damage, the reflectance and derived values of the complex dielectric constant should be regarded only as approximate in magnitude. The effective number of electrons contributing to transitions up to photon energy $\hbar\omega$ is found from the sum rule

$$n_{\text{eff}}(\omega)=\frac{2}{\pi}\frac{m}{4\pi Ne^2}\int_0^{\omega}\omega'\epsilon_2(\omega')d\omega' , \qquad (1)$$

where N is the BeF_2 molecular subunit density and m is the free-electron mass. As shown in Fig. 1(d), n_{eff} reaches a value of 9 at 40 eV and approaches 12 at 100 eV. Within a BeF_2 subunit, there are 12 valence electrons at a binding energy near 17 eV, and four more electrons in the fluorine $2s$ level with a binding energy of about 40 eV. The beryllium $1s$ and fluorine $1s$ electrons are all deeper than 100 eV. Thus n_{eff} is found to be roughly 80% of what should be expected, suggesting that the magnitude of the ϵ_2 spectrum may be low by about this amount. This is certainly within expected uncertainty in the data. The small feature in ϵ_2 between 11 and 12 eV is dependent on choice of extrapolation parameters and seems to be an artifact of the assumptions made in the analysis.

The reflectance of BeF_2 glass at near-grazing incidence (85° to normal) is shown in Fig. 2 over the range 40–160 eV, encompassing the Be^{2+} K edge. The plot resulting from Kramers-Kronig analysis for non-normal incidence[9] is presented in Fig. 2(b) an expanded energy scale around 120 eV. In order to match the optical constants at lower energies deduced from Fig. 1, and in view of higher expected reflectance above the critical angle if the surface were smooth, the measured reflectance in Fig. 2(a) was multiplied by a factor of 2 before the inversion leading to Fig. 2(b). This affects primarily the magnitude of ϵ_2 and not the peak energy. While the magnitudes of the reflectance and derived dielectric constants are thus very approximate, the main purpose in Fig. 2 is to obtain the energy of the dominant optical resonance at the Be^{2+} K edge. The

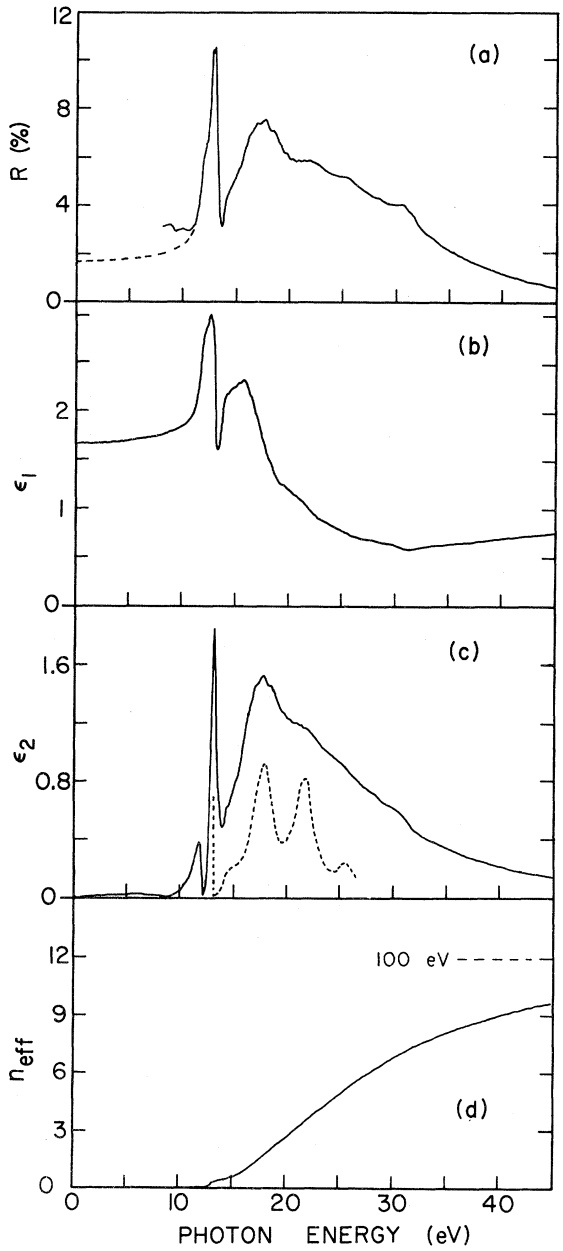

FIG. 1. (a) Reflectance of BeF_2 glass at near-normal incidence from 8 to 45 eV. Dashed line shows the low-energy extension assumed for Kramers-Kronig analysis. Analysis yields approximate values for ϵ_1 and ϵ_2, shown as solid lines in (b) and (c). Effective number of electrons per BeF_2 molecular unit, computed from the sum rule in Eq. (1), is plotted vs photon energy in (d). Dashed curve in (c) is a theoretical $\epsilon_2(\omega)$ spectrum (arbitrary normalization) discussed in the text.

wavelength calibration of the monochromator was checked against known transmission edges of thin films of beryllium[10] and aluminum.[11] The uncertainty in photon-energy calibration in the neighbor-

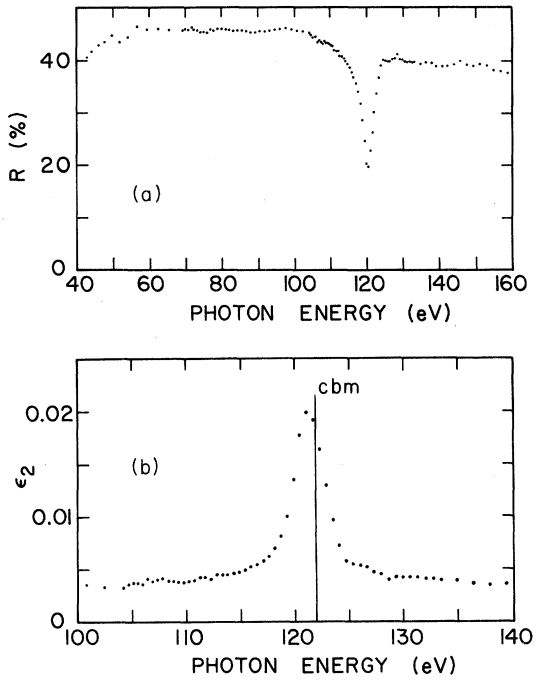

FIG. 2. (a) Reflectance of BeF_2 glass at grazing incidence (85° to normal) from 40 to 160 eV. (b) Approximate ϵ_2 spectrum from Kramers-Kronig analysis of the reflectance data. Line at 121.9 eV indicates the energy separation of the Be^{2+} 1*s* core level and the Γ_1 CBM deduced from photoelectron and optical gap data as described in the text.

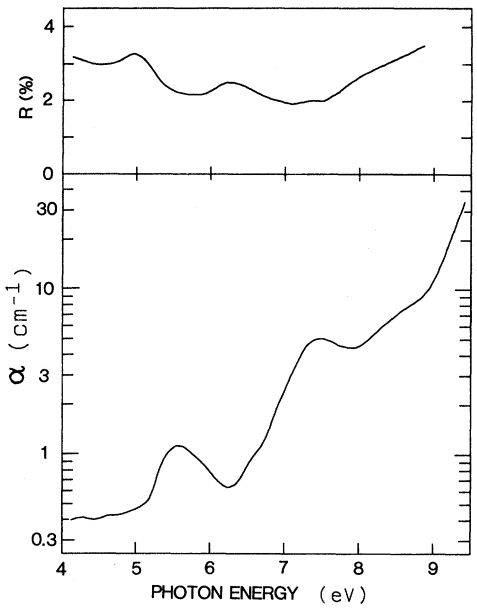

FIG. 3. Reflectance of a BeF_2 glass sample at near-normal incidence from 4 to 9 eV. Optical-absorption coefficient of the same glass sample, after correcting for surface-related losses, is shown in the lower part.

hood of 120 eV is less than 0.4 eV.

The absorption coefficient α and reflectance R of a relatively high-purity sample of BeF_2 glass are shown in Fig. 3 over the spectral range 4—9.5 eV. Substantial attenuation, on the order of 20%, is associated with the surfaces of the prepared samples. The absorption coefficient in Fig. 3 is derived from measurements on two samples of the same glass, 0.074 and 0.549 cm thick. Thus if surfaces of the two samples are assumed to be identical, effects of reflectance, diffuse scattering, and near-surface absorption can be eliminated, so that the quantity α plotted in Fig. 3 is representative of bulk optical attenuation in the glass.

Figure 4 shows a photoelectron energy-distribution curve for BeF_2 glass under excitation by 50-eV photons. Also shown for comparison are photoelectron spectra for crystalline CaF_2 and SrF_2 measured under the same conditions. The tendency for positive charging of the insulating samples was counteracted by a filament operating as a source of low-energy electrons. Under conditions of constant incident photon flux and constant filament current, a given sample equilibrated at a small, typically negative, potential, shifting the entire emitted-electron spectrum rigidly relative to vacuum energy. Some feature of the spectrum must be established as an energy reference, and then energies of all other features can be determined relative to it. We choose as reference (zero energy) the prominent valence (F^- 2*p*) peak in each material. The actual energies of these peaks in the measured spectra were between 40 and 50 eV, depending on several factors such as total photoelectron yield and location of the sample relative to the filament. Energy separations of valence and core levels obtained in this way are in good agreement with measurements on thin evaporated films of CaF_2 and SrF_2,[4] where charging is much less of a problem.

B. Crystalline BeF_2

Glass starting material was crystallized in the α-BeF_2 phase as described in the discussion of experiment. Whereas BeF_2 glasses had been prepared as highly transparent samples with moderate surface polish, the obtainable crystalline BeF_2 samples are better described as translucent and large grained, with a dull surface finish. Our reflectometer had no provision for angle-integrated measurements. The measured specular reflectance of the crystalline BeF_2 sample shown in Fig. 5 is very low, about 1.8% at the peak. While the data are thus not

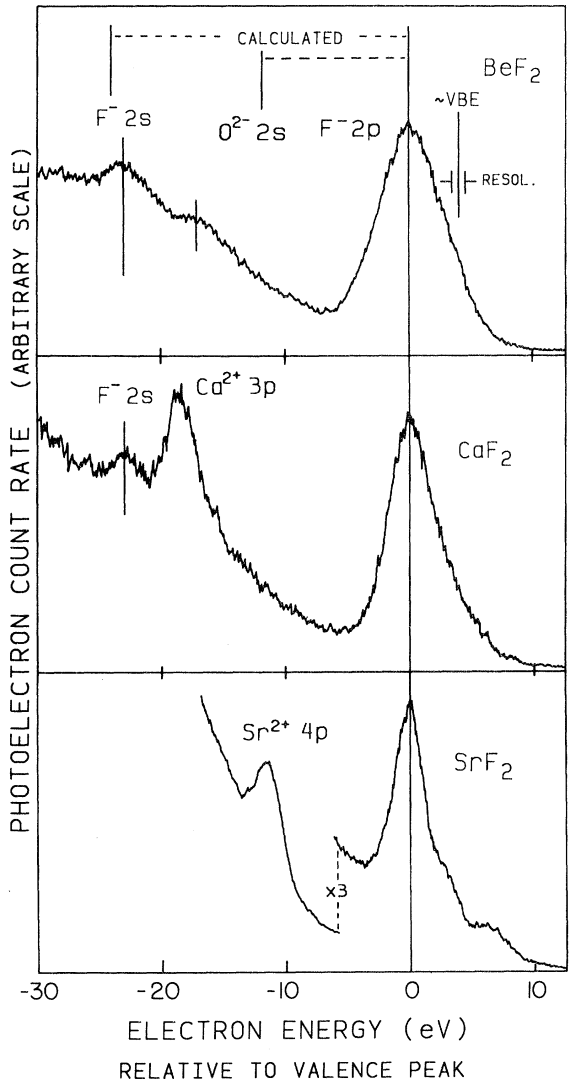

FIG. 4. Energy-distribution curves of photoelectrons emitted from bulk insulating samples of vitreous BeF_2, crystalline CaF_2, and crystalline SrF_2 under 50-eV photon excitation. Sample charging was balanced by an electron-flood source (filament) so that the scale of detected electron energy may be shifted electrostatically. Therefore, energies are displayed relative to the F^- $2p$ valence-band peak in all cases. Samples were argon-sputter-etched before measurement.

analyzable for optical constants, the basic structure of a sharp peak below a shoulder on a broader peak is clearly discernible. On comparison to the reflectance of BeF_2 glass, the basic features are seen to occur at very nearly the same energies. In particular, the sharp reflectance peak is at 12.9 eV in the crystal, compared to 12.8 eV in the glass, which is almost within the uncertainty of defining the peak

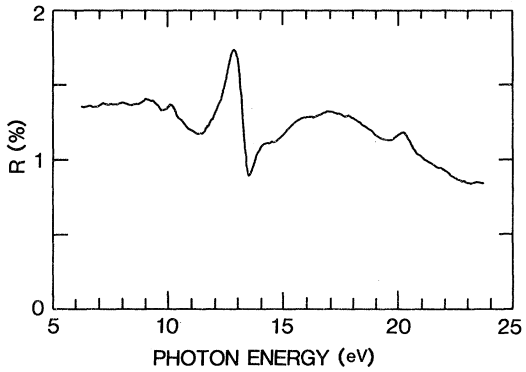

FIG. 5. Measured reflectance at near-normal incidence from a sample of crystalline α-BeF_2. Low reflectance magnitude is a result of diffuse scattering from attainable sample surfaces, as measured by a detector of limited area.

energy. This is similar to observations on vitreous and crystalline SiO_2.[12]

IV. METHOD OF CALCULATION

The electronic structure of bulk beryllium fluoride is calculated within the cluster model. The energy levels calculated in this manner form a density of states which is consistent with that of energy-band theory, provided that one uses a large enough cluster and that one applies the proper boundary conditions.[13] Application of this model to BeF_2 has been discussed in Ref. 5. Beryllium fluoride is an ionic material composed of Be^{2+} and F^- ions, and occurs in many of the same crystal structures as silica (SiO_2), in particular the α-quartz and β-crystobalite structures. The basic building block is the BeF_4 tetrahedron. In the case of silica, the electronic structure is determined mainly by the SiO_4 tetrahedron, and is fairly insensitive to the particular long-range crystal structure.[14–16] We expect this behavior to carry over to the case of BeF_2, and feel justified in using the cluster model which has successfully reproduced the state densities of band theory for SiO_2 (Ref. 17) as well as for ionic materials such as NaF and LiF.[18] We have studied here the idealized β-crystobalite (cubic) structure as it is the simplest, that is it has the highest symmetry, of any of the structures in which BeF_2 is found. Use of the cluster model has the disadvantage of not giving the dispersion of the energy bands in $\vec{k}$ space, but it conveniently allows for a simple treatment of defects and impurities in the crystal.

The clusters chosen to study the idealized crystal were the Be_2F linear "molecule" and the BeF_4 tetrahedron, both of which were embedded in the proper crystalline electrostatic potential. These two

clusters together allow for the study of each ion in the presence of its nearest neighbors, and also provide the necessary information about the crystal symmetry of the electronic wave functions. Vacancy and impurity-ion states have also been studied, in particular the anion vacancy, a carbon ion substituted for a beryllium ion, and an O^{2-} ion substituted for a fluorine ion with a neighboring fluorine vacancy to conserve local charge neutrality. For the anion-vacancy and substitutional carbon-ion calculations, the clusters used included the nearest-neighbor ions and the electrostatic potential of the extended crystal. For the case of oxygen substituted for two fluorine ions, there are two high-symmetry geometries possible. In one, the oxygen ion simply replaces a fluorine ion, with a neighboring fluorine vacancy. For the second high-symmetry geometry, the oxygen ion is positioned midway between the two fluorine vacancies. Both geometries have been studied, using clusters which included the nearest beryllium ions and the Madelung potential due to the remaining crystal.

The calculations presented here were performed within the *ab initio* unrestricted Hartree-Fock (UHF) approximation. The many-body Hamiltonian is

$$H=-\tfrac{1}{2}\sum_i \nabla_i^2-\sum_{i,I}\frac{Z_I}{|\vec{r}_i-\vec{R}_I|}+\tfrac{1}{2}\sum_{\substack{i,j\\ i\neq j}}\frac{1}{|\vec{r}_i-\vec{r}_j|}+\tfrac{1}{2}\sum_{\substack{I,J\\ I\neq J}}\frac{Z_I Z_J}{|\vec{R}_I-\vec{R}_J|}\,. \tag{2}$$

The UHF wave function is the antisymmetrized product of one-electron orbitals of the form

$$\Psi=\mathscr{A}(\phi_1\alpha\phi_2\alpha\cdots\phi_n\alpha\phi_{n+1}\beta\cdots\phi_m\beta)\,, \tag{3}$$

where we have used atomic units: $e=\hbar=m=1$, length in bohr (1 bohr=0.529 Å), and the energy in hartrees (1 hartree=27.2 eV). The UHF wave function of Eq. (3) differs from the usual restricted Hartree-Fock wave function in that the spin-up–spin-down electron pairs are not required to have the same spatial wave function ϕ. Also, the orbitals ϕ_i are not explicitly required to have the symmetry properties of the crystal, although in practice they usually are approximate eigenfunctions of the crystal-symmetry operators.

The Hartree-Fock one-electron energy levels have a well-known deficiency in that the calculated band gap is too wide. Here we have used a static Mott-Littleton-type correction to include long-range polarization effects,[19] and the self-consistent technique of Pantelides *et al.*[20] to include local relaxation effects to correct the Hartree-Fock energy levels. These correlation corrections to the Hartree-Fock approximation employ no adjustable parameters and have been discussed extensively in the literature,[20,21] where they have been shown to produce accurate energy levels in the sense of agreement with experiment.

Excitonic states are studied here by modifying the sum over occupied orbitals to include those orbitals occupied in the excited-state configuration, rather than summing over the lowest-energy orbitals as in the ground state. The difference in total energy ΔE_{SCF} (where SCF is the self-consistent field) between the ground-state electronic configuration and an excited-state configuration with one electron promoted from an otherwise occupied valence band to a previously unoccupied conduction band is the energy to create an exciton. Both the local electronic relaxation and the electron-hole interaction are treated nonempirically by this type of calculation in a totally self-consistent manner. We note also that long-range correlation effects tend to cancel each other when taking an energy difference.[20] In creating an exciton there is not a major change in the electronic charge distribution in the solid, and hence the long-range correction is essentially the same for the two configurations.

The one-electron orbitals are described with a set of Cartesian Gaussian basis functions. The basis sets used were derived from the atomic sets of Huzinaga,[22] contracted to valence double-zeta accuracy, with diffuse *p*- and *d*- type polarization functions then added. All basis contractions were performed with each ion in the presence of the crystalline Madelung potential. The integrals and UHF programs were written by A. B. Kunz. All integrals are calculated exactly to the precision of our computer (7.5 significant figures), and the UHF calculations were performed to a required self-consistency in total energy of 10^{-4} hartree.

V. THEORETICAL RESULTS

The occupied Hartree-Fock valence energy levels for BeF_2 in the (idealized) β-crystobalite structure have been reported previously by one of the present authors,[5] and are reproduced here for convenience in Fig. 6. The valence bands are found to be made up of fluorine $2p$ orbitals, with a band width of 5.8 eV. A Mulliken population analysis of the wave function shows the solid to be nearly perfectly ionic. The gap between the occupied orbitals (valence bands) and the virtual orbitals (conduction bands) is 16.0 eV. The valence-band energy levels are grouped

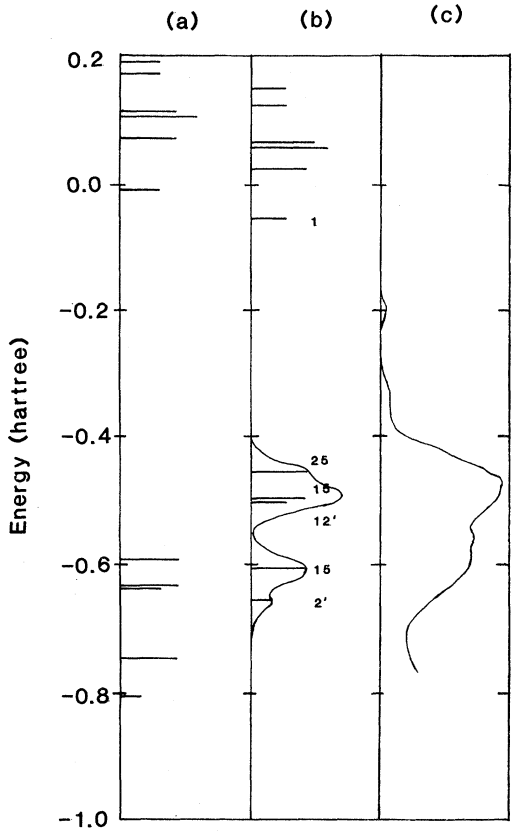

FIG. 6. Shown here are the one-electron energy levels for BeF_2 in the β-crystobalite structure, determined from the appropriate combination of the electronic energy levels for the two clusters discussed in the text. These are calculated within the Hartree-Fock approximation (a). Heights of the lines shown correspond to the degeneracy of the orbitals. Effects of correlation corrections have been included in (b). Symmetry labels for the wave functions are also given. Results can be compared to photoemission spectra of Ref. 4, reproduced in (c). Here we have shifted the zero of energy (the vacuum level) such that the valence bands approximately line up.

into two types which have the symmetry properties of bonding and nonbonding orbitals, just as in the SiO_2 electronic structure. The splitting between the two groups is about 3.5 eV. This valence-band gap is not clearly resolved in the UPS data of Poole *et al.*[4] [Fig. 6(c)], but two peaks do appear in this spectrum with a splitting of about 3.2 eV. In a sample of lower crystal symmetry than β-crystobalite and particularly in the amorphous solid, one expects this splitting to be smeared out and the mid-band gap filled because of the lower symmetry of the crystal field. This effect is well established in comparing the valence-band state densities of crystalline and amorphous silica.[14] Dispersion of the energy bands in $\vec{k}$ space, not included in our calculation, will also cause the energy levels to broaden.

The most prominent effect of including correlation corrections is to narrow the band gap. These corrections raise the valence-band energies by 3.5 eV and lower the virtual (conduction) energy levels by 1.8 eV. Thus the energy-level scheme of Fig. 6(b) is derived, with a band gap of 10.7 eV. As an aid in comparing the calculated energy levels with experiment, the effects of dispersion in $\vec{k}$ space have been approximated by giving each energy level a Gaussian profile of 0.7 eV [full width at half maximum (FWHM)]. The resulting approximation to the valence-band density of states [Fig. 6(b)] can be compared to the reported photoemission spectrum of evaporated BeF_2 films by Poole *et al.*[4] shown in Fig. 6(c). The present calculation places the F 2*s* level at -39.1 to -39.7 eV with respect to the vacuum, or ~ 28 eV below the top of the (Gaussian-broadened) valence bands. The splitting in this level is due to the crystal field. This energy value is in good agreement with the UPS data presented in Fig. 4, which show a peak at 27 eV below the top of the valence band. Poole *et al.* have reported an x-ray photoelectron spectroscopy (XPS) measurement[4] which places the beryllium 1*s* core level 122 eV below the vacuum. The present calculation places this level at -126 eV, after correlation effects are added to the Hartree-Fock energy.

From inspection of the expansion coefficients and the degeneracies of the calculated electronic wave functions, we have determined the symmetry types (see Table I) of the one-electron orbitals (which become bands when extended throughout $\vec{k}$ space). The symmetry labels corresponding to the center of the Brillouin zone for this crystal structure are given for the valence orbitals in Fig. 6(b). The analogies which have been made with the electronic structure of silica are well founded as the valence-band ordering for BeF_2 (see also Ref. 5) is exactly the same as the band ordering reported by Schneider and Fowler[15] for SiO_2 in the same crystal structure. This result is what one would expect from group-theoretical considerations, from which the crystal structure is known to be the dominant factor in determining the band order.[23] Of particular importance here is that the lowest-energy transition across the band gap ($\Gamma_{25} \rightarrow \Gamma_1$) is optically forbidden. The lowest energy for an allowed transition is 1.2 eV greater in energy, from Γ_{15} to Γ_1, giving an optical band gap of 11.9 eV. The cluster model employed here does not give us information about the dispersion of the energy bands in $\vec{k}$ space, and we therefore cannot exclude the possibility of an indirect transition of lower energy. The optical excitation of such a transition would, of course, have a greatly reduced matrix element as it would require the partici-

TABLE I. Breakup of symmetry types into basis-function contributions as deduced from group-theoretical considerations is shown for the β-crystobalite crystal structure. The order of the valence levels and lowest two conduction levels given here is that which was calculated using the UHF cluster technique described in the text.

Orbital symmetry-type at Brillouin-zone center	Degeneracy	Basis contributions Be^{2+}	Basis contributions F^-	Molecular-bond description
Γ_{25}'	3	$d_{xy,xz,yz}$		Antibonding conduction levels
Γ_1	1	s	s	
Γ_{25}	3	f	$p_{\text{tangential}}$	Nonbonding valence levels
Γ_{15}	3	p	$p_{\text{tangential}}$	
Γ_{12}'	2	$d_{z^2-1/3r^2}^{x^2-y^2}$	$p_{\text{tangential}}$	
Γ_{15}	3	p	p_{radial}	Bonding valence levels
Γ_2'	1	s	p_{radial}	

pation of a phonon.

Using the ΔE_{SCF} technique described in Sec. IV, we have self-consistently calculated the excitonic transition energy. For the lowest-energy transition, from the uppermost valence level Γ_{25} to the lowest conduction level Γ_1 (which is an optically forbidden transition), this energy is found to be 11.7 eV. The lowest-energy optically allowed excitonic transition is from the second-highest valence level Γ_{15} to the lowest conduction level Γ_1 and is found to be 12.9 eV, in excellent agreement with the experimental value.

The Hartree-Fock energy levels are not accurate in the sense that correlation effects are not included. Corrections for this have been included here in an approximate way, but the errors are still fairly large, as can be seen by comparing the theoretical value for the allowed band gap of 11.9 eV with the experimental value of 13.8 eV. It is important to note here that the errors in the energy separations of the occupied valence levels (intraband features) are an order of magnitude smaller than those of interband features such as the band gap. Thus none of these errors will have any effect on the band ordering, and the lowest-energy transitions across the gap will remain optically forbidden. Electronic correlation corrections to the Hartree-Fock value have not been included in the calculation of the exciton transition energy as the corrections to a calculated transition energy would be quite small.[20] This can be understood intuitively because most of the correlation energy is the same for the two electronic configurations, and thus this contribution will tend to cancel when the energy difference is taken. We also note that systematic errors in the computation of the electronic energy levels will cancel when the difference in total energies is taken. The calculated excitonic transition energy is thus expected to be more accurate than the calculated band gap.

In order to compare the present calculation of the electronic structure of BeF_2 with reflectance measurements, we need to calculate the imaginary part of the dielectric constant for optical (zero momentum transfer) transitions. The calculated energy dependence of $\epsilon_2(\vec{q}=0,\omega)$ is shown by the dashed line in Fig. 1(c). For the purposes of comparison with experiment, we have adjusted the energy of the lowest allowed band-to-band transition to be 1 eV ($\sim$ exciton binding energy) higher than the calculated energy of the allowed exciton, giving an optical band gap of 13.9 eV.

We have also calculated the energy levels of several impurities in the BeF_2 crystal, including the anion vacancy and substitutional carbon and oxygen ions. These energy levels are shown in Fig. 7. We note that the substitutional carbon ionizes to C^{4+} in the geometry we have assumed, which has been described above. A geometry which might be expected to have a lower total energy is one where the carbon impurities, known to exist in quantities of 4 at. % in BeF_2 samples,[3] are found in the CO radical, which we have not investigated. Since the BeF_2 crystal structure is not very dense, there is no difficulty in spatially accommodating such a large impurity. Of the two high-symmetry geometries studied here, the oxygen impurity is energetically most stable replacing a fluorine ion, with a neighboring fluorine vacancy to conserve local charge neutrality. This geometry is reasonable based on chemical considerations as oxygen ions prefer a twofold coordination. The valence energy levels for the oxygen impurity are shown in Fig. 7; there are both occupied

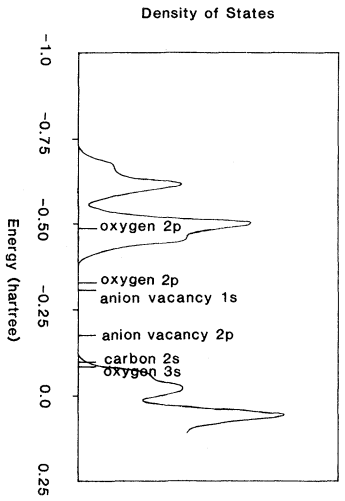

FIG. 7. Correlated density of states with impurity levels indicated is shown.

(2*p*) and unoccupied (3*s*) states in the gap. The oxygen 2*s* level is placed by the present calculation at −27.1 eV, or 14.7 eV below the top of the valence band, after the Hartree-Fock eigenenergies are corrected for correlation effects. These eigenenergies would be modified if the oxygen ion were found as a constituent of the OH^- or CO radicals.

VI. DISCUSSION

A. Valence structure

The theoretical results presented above indicate that the minimum-energy band-to-band transition in (β-crystobalite structure) BeF_2 is from a valence band labeled Γ_{25} at the Brillouin-zone center to the conduction band labeled Γ_1. The transition is optically forbidden. Attributing the minimum band gap to a direct transition at the Brillouin-zone center is an assumption based on analogy to the band-structure calculations for SiO_2 by Schneider and Fowler.[16] It must be noted, however, that there remains some uncertainty over whether the band edge is direct or indirect in SiO_2 and, by implication, in BeF_2 also. As noted above, the present cluster calculations do not address this issue, but do establish that the ordering of the valence bands and lower conduction bands in BeF_2 is the same as in SiO_2.

The peak in ϵ_2 associated with the 12.8-eV reflectance peak in Fig. 1 is at 13.0 eV. This resonance is the lowest exciton at the allowed optical gap connecting the Γ_{15} valence band and the Γ_1 conduction band. It follows from the above considerations that this 13-eV peak is degenerate with conduction states if the valence-band splitting exceeds the exciton binding energy. Such is the case for the prominent 10.3-eV peak in SiO_2,[24] since the photoconductivity threshold is 8.9 eV,[25] generally accepted as the forbidden minimum band gap. Photoconductivity measurements have not yet been performed on BeF_2 to our knowledge.

An approximate theoretical ϵ_2 spectrum, discussed above, is superimposed on Fig. 1(c), as shown with dashed lines. The calculated exciton energy at the Γ_{15}-Γ_1 allowed band gap is in excellent agreement with experiment. The four major features between 13 and 30 eV are also in agreement with peaks in the calculated ϵ_2 spectrum. The threshold near 14 eV results from band-to-band transitions from the upper Γ_{15} valence states. The 17-eV peak includes contributions from the lower Γ_{15} states to Γ_1. Above this, transitions to higher conduction bands begin to contribute, and no simple assignment of features can be made. The experimental peak corresponding to the calculated 25-eV peak is hardly visible in ϵ_2, but can be seen readily in the reflectance.

B. Beryllium *K* edge

In recent years there has been substantial interest in core excitons in the alkali halides. Lithium halides have been widely studied because of the experimental accessibility of the Li *K* edge near 60 eV and the simplicity of the alkali-metal—ion core. There is typically observed a strong absorption peak at about 2 eV lower energy than the band-to-band threshold identifiable from XPS and the optical band gap. Since the transition from the Li^+ 1*s* core to the Γ_1 conduction-band minimum (principally Li^+ 2*s*) is dipole forbidden, the lowest exciton associated with the core threshold should be optically forbidden. Pantelides[26] and Kunz[27] have pointed out that the Coulomb potential of the hole in the alkali-metal *K* shell is hardly screened at all and can mix band states over the range of 10—13 eV, accounting for the strong excitonic peak typically observed below the band-to-band threshold.

While core excitons have been studied in many of the alkali halides, there has been comparatively little done in this area with the alkaline-earth halides. Observations of a Ca^{2+} *K* core exciton in the x-ray absorption spectrum of CaF_2 was reported recently.[28] A small peak was found about 3.2 eV below the band-to-band threshold. This is a somewhat larger energy difference than is typically found in alkali halides. On the other hand, the relative strength of the exciton peak was lower than in the alkali halides. BeF_2 affords an opportunity among alkaline-earth halides similar to LiF among alkali halides, in that the constituent ions are very light

and the Be^{2+} K shell is accessible to ordinary vacuum-ultraviolet spectrometers.

Poole *et al.* have determined from photoelectron spectroscopy that the Be^{2+} $1s$ shell lies 105.3 eV below the centroid of the F^- $2p$ valence states.[4] Their measurements of the valence-band spectrum place the valence-band edge about 4 eV higher than the band centroid. Reflectance data place the allowed (Γ_{15}-Γ_1) optical gap at 13.8 eV. The calculations discussed above indicate that the Γ_{25}-Γ_1 forbidden gap is about 1.2 eV lower, at 12.6 eV. The latter gap is the one we should use in this case, since transitions from Γ_{25} to the high-lying plane-wave-like final states obtained in the photoelectron data should be allowed and will constitute the top edge of the ultraviolet photoelectron spectrum. Thus the energy difference between the Be^{2+} $1s$ core and the conduction-band minimum (CBM) is

$$\Delta E(Be^{2+}\ 1s-\text{CBM})=105.3+4.0+12.6\ \text{eV}$$
$$=121.9\ \text{eV}\ . \qquad (4)$$

Poole *et al.* measured the binding energy of Be^{2+} $1s$ to be 122.5 eV below vacuum energy.[4] The difference in these two energies implies an electron affinity of roughly 0.6 eV in BeF_2, in reasonable agreement with electron affinities in other wide-gap halide crystals, although the uncertainty in this determination is about ± 0.8 eV.

The grazing-incidence reflectance of BeF_2 in Fig. 2 exhibits a dip centered at 120.3 eV. At grazing angles for which total external reflection occurs, such a dip results from an absorption resonance causing a peak in the refractive index. An approximate Kramers-Kronig analysis for non-normal incidence[9] places the peak in ϵ_2 at 121.3 eV. On subtracting from the interband threshold energy deduced earlier, we find that the core-exciton absorption resonance occurs ~ 0.6 eV below the conduction-band minimum, which is within the overall uncertainty in the quantities subtracted, i.e., ± 1 eV.

The appearance of the ϵ_2 spectrum in Fig. 2 is quite similar to the Li^+ K-edge absorption spectrum in LiF, in which a single strong peak somewhat below the core-level—to—conduction-band threshold dominates the edge spectrum. It is mildly surprising that the peak does not occur as far below the CBM in BeF_2 as in LiF and CaF_2. The calculations presented above indicate that the lowest Γ_{15} conduction state lies only about 3 eV above the Γ_1 CBM in BeF_2. Even granting that calculations of the higher conduction states are uncertain, this is substantially lower than the (10—13)-eV separation of s- and p-like conduction states in LiF.[26,27] Thus if we attempt to describe the main peak as the lowest effective-mass exciton state bound to the high-lying Γ_{15} conduction band, we must account for the change from a 10-eV binding energy in LiF to a 5-eV binding energy in BeF_2. Conversely, if we describe it as an exciton with an $n=2$, p-like envelope function, bound to the Γ_1 minimum in an effective-mass picture, the inferred binding energy is again about half as large as in LiF,[27] and perhaps $\frac{1}{3}$ as large as in CaF_2.[28]

In the first place, these comparisons may simply emphasize the point that effective-mass pictures should not be taken seriously with regard to the alkali-metal core excitons.[26] It remains an interesting question, however, why the Be^{2+} K core-exciton peak is located so much closer to the inferred CBM and the nearest calculated p-like density of final band states than in the alkali-halide cases and the single other known alkaline-earth halide case. Our determination rests crucially on relative accuracy of the valence and core binding energies measured by Poole *et al.*[4] They state their uncertainty in determining binding energies to be 0.1 eV, and so it does not seem likely that a (3—5)-eV energy difference can be blamed entirely on experimental differences. BeF_2 has a structure not shared by any of the other halide crystals. It has a very small cation-anion nearest-neighbor distance of 1.54 Å as compared, for example, with 2.01 Å in LiF. There could thus be significant differences in core-hole screening because of the greater intrusion of the F^- charge clouds in the vicinity of the Be^{2+} ion, though we have no other evidence at present regarding screening.

C. Impurities and other defects

The reflectance and absorptance below the band edge, from 4 eV to about 9.5 eV, are shown for a sample of BeF_2 glass in Fig. 3. One expects the absorptance in this region of the spectrum to be variable from sample to sample, and such is the case experimentally. The glass which yielded the data of Fig. 3 was one of the best nominally pure BeF_2 samples from the point of view of ultraviolet transparency. Other samples become opaque ($\alpha \approx 30$ cm^{-1}) at about 8.5 eV. Impurity absorption is obviously present. Transmission in the ultraviolet is affected by the presence of oxygen[29] and hydroxyl groups.[30] The apparent uv edge is also affected by Zr, Al, Si, and Fe, which were present in concentrations $\gtrsim$ 100 ppm. Dumbaugh and Morgan reported optical transmission up to 10.2 eV in certain mixed compositions, such as 70 at.% BeF_2, 10 at.% AlF_3, 10 at.% KF, and 10 at.% CaF_2. They suggested that since these mixed-composition glasses have a lower effective melting temperature and higher density, less carbon from the crucible would be incor-

porated in the glass.[30] Griscom *et al.* have suggested that ultraviolet transmission in some BeF_2 glasses prepared in a nickel distiller to remove water may be limited by scattering from small nickel-ferrite inclusions.[31]

Approximate calculated energies for the F band ($1s$-$2p$ transition of an electron trapped at a fluoride vacancy) and oxygen impurity ($2p\pi \rightarrow 3s$ transition) in BeF_2 can be deduced from Fig. 7. Comparing the calculated F band at 4.9 eV and the oxygen-impurity band at 7.2 eV with the absorption peaks in Fig. 3 suggests possible candidates for the responsible defects, although a correlation has not been established. When detailed experiments on defects in BeF_2 are undertaken, these calculated energy levels should be a useful guide.

Photoelectron spectra for evaporated films of the alkaline-earth fluorides have been measured by Poole *et al.*[4] Because the samples were thin films on conducting substrates, charge buildup was not a serious problem, and quantitative binding energies could be measured. Binding energies and widths of the F^- $2p$ and Be^{2+} $1s$ peaks in BeF_2 were determined, but the F^- $2s$ peak was not measured. In order to determine the binding energy of the F^- $2s$ level in BeF_2 for comparison to theory, to compare UPS valence-band structure in a bulk glass sample with that in a thin film of BeF_2, and to look for impurity or defect levels in the glass we have measured photoelectron energy-distribution curves from BeF_2 glass. The samples were highly insulating and required charge-neutralization procedures as described above. The data of Poole *et al.* still provide the only absolute binding energies available. By referencing our data to the valence-band peak, we can use valence binding energies from Ref. 4 to determine indirectly the binding energies of deeper levels.

The energy-distribution curves produced by 50-eV photons are shown in Fig. 4 for vitreous BeF_2. Data for crystalline CaF_2 and SrF_2 measured in the same apparatus are shown for comparison. A peak located 23 eV below the F^- $2p$ peak in BeF_2 is attributed to transitions from the F^- $2s$ core level. This identification is made partly by comparison to the F^- $2s$ peak in CaF_2 and partly on the basis of agreement with our calculated F^- $2s$ energy. Combined with the F^- $2p$ binding energy of 17.2 eV,[4] the present data yield the binding energy of the F^- $2s$ level in BeF_2 as 40.2 eV.

Another small peak lies 17 eV below the valence-band centroid, or about 34.2 eV below vacuum energy. There are no anticipated intrinsic levels in BeF_2 which should have a binding energy near 34 eV, since F^- $2s$ has already been attributed to the 40.2-eV level, and its energy bandwidth is expected to be much smaller than 6 eV. Thus we attribute the photoelectron peak at 34-eV binding energy to an impurity. Oxygen is a known impurity in our BeF_2 samples,[3] so the oxygen $2s$ level is a reasonable candidate for the feature in question. The calculated O^{2-} $2s$ energy is shown in Fig. 4 for comparison.

The UPS valence-band spectrum measured by Poole *et al.*[4] exhibited a pronounced shoulder. Such a shoulder is in agreement with the computed valence bands for the β-crystobalite structure reported by Bedford[5] but is not observed in the spectra of Fig. 4. The data for SrF_2, obtained under identical conditions, are presented to verify that finer structure can be measured by the methods described. We thus attribute the lack of structure in our valence-band UPS spectrum to the state of the sample, i.e., that it was a glass, that it contained more near-surface impurities than the evaporated film in Ref. 4, or that the argon-sputter-etching required to clean the bulk samples produced large numbers of defect states. All three factors are probably present to some degree. The effect of sputter-cleaning alkaline-earth halide samples is severe. We attribute the structure above the valence band of SrF_2 in Fig. 4 to effects of argon-ion sputtering. Auger-sputter-profiling of BeF_2 glass showed that the surface stoichiometry changes very rapidly during ion etching.[3] In the face of this uncertainty over effects of sputtering, it does not seem possible to reach a conclusion from present data about the valence-band shape in bulk BeF_2 glass. The energy marked VBE in Fig. 4 is the approximate valence-band edge relative to the F^- $2p$ centroid, deduced from the data of Ref. 4. The tail to higher energy is presumed due to disorder and impurities not found in the evaporated films.

VII. CONCLUDING REMARKS

We have made substantial use of the SiO_2 analog in trying to understand the BeF_2 data. The analogy seems to hold up in regard to a wide variety of phenomena in the two materials, even though one is highly ionic and the other exhibits substantially covalent bonding. Continuing detailed comparison of the two materials should yield insight into both. In particular, a comparative study of ionizing radiation damage in suitably pure BeF_2 and SiO_2 will be very useful.

Although beryllium fluoride does not have as large a band gap as preliminary indicators such as visible refractive index and dispersion or valence binding energy had implied, it still has potential as an ultraviolet optical material. The usefulness of BeF_2 relative to LiF and other materials will depend on the ability to prepare purer bulk glasses, good-quality films, and large single crystals. Its

radiation-damage properties and the degree to which its surfaces can be protected from attack by atmospheric moisture will also determine its ultimate usefulness.

ACKNOWLEDGMENTS

We wish to thank M. N. Kabler, W. B. Fowler, and R. S. Weidman for helpful discussions. The contributions of D. J. Nagel and P. H. Klein to investigations leading up to this study are gratefully acknowledged. We wish to thank the NBS Synchrotron Ultraviolet Radiation Facility and its staff for beam time and assistance. The work of M. J. W., D. D. K., and C. F. C. was performed under the auspices of the Division of Materials Sciences of the U. S. Department of Energy, Office of Basic Energy Sciences. K. L. B. acknowledges support from the National Research Council.

---

*Also at: Sachs-Freeman Associates, Inc., Bowie, MD 20715.

[1]M. J. Weber, C. F. Cline, W. L. Smith, D. Milam, D. Heiman, and R. W. Hellwarth, Appl. Phys. Lett. 32, 403 (1978).

[2]S. H. Wemple and M. DiDomenico, Jr., Phys. Rev. B 3, 1338 (1971); S. H. Wemple, Appl. Opt. 18, 31 (1979).

[3]R. T. Williams, D. J. Nagel, P. H. Klein, and M. J. Weber, J. Appl. Phys. 52, 6279 (1981).

[4]R. T. Poole, J. Szajman, R. C. G. Leckey, J. G. Jenkin, and J. Liesegang, Phys. Rev. B 12, 5872 (1975).

[5]K. L. Bedford, Solid State Commun. (in press).

[6]C. F. Cline and M. J. Weber, Friedrich-Schiller-University Report No. 28 [also available at Lawrence Livermore Laboratory, Livermore, California as report NO. UCRL-81168 (unpublished)]; C. F. Cline, D. D. Kingman, and M. J. Weber, J. Non-Cryst. Solids 33, 417 (1979).

[7]D. L. Ederer, B. E. Cole, and J. B. West, Nucl. Instrum. Methods 172, 185 (1980).

[8]B. W. Veal and A. P. Paulikas, Phys. Rev. B 10, 1280 (1974).

[9]D. M. Roessler, Brit. J. Appl. Phys. 16, 1359 (1965).

[10]T. A. Calcott, E. T. Arakawa, and D. L. Ederer, Jpn. J. Appl. Phys. 17, Suppl. 17-2, 149 (1978).

[11]K. Codling and R. P. Madden, Phys. Rev. 167, 587 (1968).

[12]H. R. Phillip, Solid State Commun. 4, 73 (1966).

[13]A. B. Kunz and D. L. Klein, Phys. Rev. B 17, 4614 (1978).

[14]S. T. Pantelides and W. A. Harrison, Phys. Rev. B 13, 2667 (1976).

[15]P. M. Schneider and W. B. Fowler, Phys. Rev. B 18, 7122 (1978); E. Calabrese and W. B. Fowler, *ibid.* 18, 2888 (1978).

[16]P. M. Schneider and W. B. Fowler, Phys. Rev. Lett. 36, 425 (1976).

[17]T. L. Gilbert, W. J. Stevens, H. Schrenk, M. Yoshimine, and P. S. Bagus, Phys. Rev. B 8, 5977 (1973).

[18]J. C. Boisvert, A. B. Kunz, and T. O. Woodruff, J. Phys. C 15, 5033 (1982); A. B. Kunz, J. C. Boisvert, and T. O. Woodruff, *ibid.* 15, 5037 (1982); J. C. Boisvert, A. B. Kunz, and T. O. Woodruff, *ibid.* (in press).

[19]N. F. Mott and M. J. Littleton, Trans. Faraday Soc. 34, 485 (1938).

[20]S. T. Pantelides, D. J. Mikish, and A. B. Kunz, Phys. Rev. B 10, 2602 (1974).

[21]W. B. Fowler, Phys. Rev. 151, 657 (1966).

[22]S. Huzinaga, J. Chem. Phys. 42, 1293 (1965).

[23]See, for example, F. Bassani and G. Pastori Parravicini, *Electronic States and Optical Transitions in Solids* (Pergamon, New York, 1975).

[24]R. B. Laughlin, Phys. Rev. B 22, 3021 (1980).

[25]T. H. DiStefano and D. E. Eastman, Phys. Rev. Lett. 27, 1560 (1971).

[26]S. T. Pantelides, Phys. Rev. B 11, 2391 (1975).

[27]A. B. Kunz, Phys. Rev. B 12, 5890 (1975).

[28]S. Muramatsu and C. Sugiura, Phys. Rev. B 26, 3092 (1982).

[29]V. D. Khalilev, Steklo. Tr. Inst. Stekla 1, 103 (1966); Tr. Gos. Opt. Inst. 39, 70 (1972).

[30]W. H. Dumbaugh and D. W. Morgan, J. Non-Cryst. Solids 38, 211 (1980).

[31]D. L. Griscom, M. Stapelbroek, and M. J. Weber, J. Non-Cryst. Solids 41, 329 (1980).